Biosensors and Bioelectronics 86 (2016) 811–817

Contents lists available at ScienceDirect

Biosensors and Bioelectronics

journal homepage: www.elsevier.com/locate/bios

# Label-free thioflavin T/G-quadruplex-based real-time strand displacement amplification for biosensing applications

Yi-Chen Du [a,c], Li-Na Zhu [b], De-Ming Kong [a,c,*]

[a] State Key Laboratory of Medicinal Chemical Biology, Tianjin Key Laboratory of Biosensing and Molecular Recognition, Nankai University, Tianjin 300071, PR China
[b] Department of Chemistry, Tianjin University, Tianjin 300072, PR China
[c] Collaborative Innovation Center of Chemical Science and Engineering (Tianjin), Tianjin 300071, PR China

ARTICLE INFO

*Article history:*
Received 3 June 2016
Received in revised form
23 July 2016
Accepted 23 July 2016
Available online 25 July 2016

*Keywords:*
Strand displacement amplification
Real-time
Sensor
G-quadruplex
Thioflavin T (ThT)

ABSTRACT

To promote application of strand-displacement amplification (SDA) techniques in biosensing, a label-free, real-time monitoring strategy for isothermal nucleic acid amplification reactions was designed. G-quadruplex structures were introduced into SDA products using specific recognition of G-quadruplexes by the fluorogenic dye thioflavin T. Performance was good for real-time monitoring of traditional SDA by a linear-amplification mechanism and for exponential cross-triggered SDA amplification. The strategy worked on a commercial real-time PCR instrument, making it suitable for biosensing platforms. As examples, two highly sensitive and specific biosensors were designed for analysis of the activity of uracil-DNA glycosylase (UDG) and the restriction endonuclease EcoRI. Detection limits were $6 \times 10^{-5}$ U/mL for UDG and 0.016 U/mL for EcoRI. Detection of corresponding targets in complex matrices such as cell lysates or human serum was also demonstrated. Compared to traditional end-point detection methods, real-time SDA-based approaches have the advantages of simple, fast operation; high sensitivity; low risk of carryover contamination; and very high throughput. The introduction of real-time monitoring strategies may promote application of SDA reactions in biosensor design.



## 1. Introduction

Nucleic acid-based biosensing platforms for various analytes have been researched over the past decades (Li et al., 2015b; Wang et al., 2014; Yamuna and Friedrich, 2011). Because nucleic acids have a unique replication property, ultrasensitive sensing systems have incorporated rational nucleic acid amplification techniques (Zhao et al., 2015). The most widely used amplification technique is polymerase chain reaction (PCR), which is powerful but has limitations (Bustin et al., 2005; Valasek and Repa, 2005). PCR requires complex thermal cycling steps for amplification and thus uses expensive instruments. PCR may not be adaptable to some biomolecular targets. Therefore, isothermal amplification techniques including rolling-circle amplification (RCA) (Chen et al., 2015b; Jiang et al., 2014; Li et al., 2015a; Zhang, et al., 2015a) and strand-displacement amplification (SDA) (Li et al., 2008, 2010) have been used to develop various sensors (Chen et al., 2015a; Huang et al., 2015). However, most of these sensing approaches still rely on the detection of the final products of the amplification reactions (Deng et al., 2008; Gao and Li, 2014; Yin et al., 2009).

Compared to end-point detection, real-time methods, in which detection of target amplification products is concurrent with amplification and performed automatically in a closed tube, offers technical advantages. These advantages include simple and fast operation; sensitive, reliable high-throughput target detection; and lack of product carryover contamination (Schmittgen and Livak, 2008; Wong and Medrano, 2005). These are advantages of real-time quantitative PCR, which converts PCR from a qualitative to a quantitative technology. Isothermal amplifications incorporating suitable real-time monitoring techniques could be adaptable to constructing nucleic acid sensors (Tian and Weizmann, 2013). Several methods are reported for real-time RCA monitoring (Jiang et al., 2013, 2015; Nilsson et al., 2002), but real-time SDA is rarely reported. One example uses of SYBR Green I dye, a fluorescent probe that is widely used in real-time PCR (Jia et al., 2010; Zhang and Zhang, 2012). However, a drawback of this method is increased background from the nonspecific response of SYBR Green I to SDA templates, primers and undesired products. SYBR Green I is not a good choice for SDA detection because SDA yields single-stranded amplification products but SYBR Green I is a

* Corresponding author at: State Key Laboratory of Medicinal Chemical Biology, Tianjin Key Laboratory of Biosensing and Molecular Recognition, Nankai University, Tianjin 300071, PR China.

http://dx.doi.org/10.1016/j.bios.2016.07.083
0956-5663/

double-stranded DNA fluorescent probe.

The discovery of noncanonical nucleic acid secondary structures allows real-time monitoring of isothermal single-stranded DNA amplification reactions. Among noncanonical nucleic acid secondary structures, G-quadruplex is attractive (Balasubramanian et al., 2011; Huang and Sen, 2015; Patel et al., 2007). Fluorescent probes that target G-quadruplexes showing highly specific signal response have been reported (Huang et al., 2014; Mohanty et al., 2013; Zhang et al., 2015b; Zhu et al., 2013). By rationally introducing G-quadruplex structure into amplification products, real-time monitoring of SDA reactions might be achieved using the specific fluorescent response of G-quadruplex probes to G-quadruplexes. This work used thioflavin T (ThT), a fluorescent dye with excellent G-quadruplex recognition specificity against other structural DNAs, as a G-quadruplex probe. A ThT/G-quadruplex-based real-time monitoring strategy was designed and the feasibility of the strategy was demonstrated in both traditional linear SDA and exponential cross-triggered SDA reactions. The superiority of real-time SDA for biosensing was demonstrated by the construction of two sensing platforms for detecting activity of uracil-DNA glycosylase (UDG) and the endonuclease EcoRI.

## 2. Experimental section

### 2.1. Materials and reagents

The oligonucleotides used in this work (Table 1) were synthesized and purified by Sangon Biotech. Co. Ltd. (Shanghai, China). Nicking endonuclease Nb.BbvCI, Klenow fragment polymerase, uracil-DNA glycosylase (UDG), endonuclease IV (Endo.IV), UDG inhibitor (UGI), restriction endonuclease EcoRI and deoxyribonucleoside 5′-triphosphate mixture (dNTPs) were obtained from New England Biolabs (Beijing, China). ThT (3,6-dimethyl-2-(4-dimethylaminophenyl) benzo-thiazolium cation) was obtained from Sigma. All chemical reagents were of analytical grade and used without further purification.

### 2.2. ThT/G-quadruplex-based SDA reactions

100 nM template (**T-1**, **T-2/T-2s** mixture) and variable amounts of primer **P** in 1 × NEBuffer 2 (50 nM NaCl, 10 mM Tris-HCl, 10 mM $MgCl_2$, 1 mM DTT, pH7.9) was incubated at 95 °C for 5 min and then allowed to cool slowly to 25 °C and incubated at 25 °C for 30 min. Next, 0.4 mM dNTPs, 5 μM ThT, 0.5 U Klenow fragment polymerase and 2.3 U Nb.BbvCI were added. Then, 30 μL of the reaction mixture was incubated at 37 °C on the ABI StepOne Plus real-time PCR system (Applied Biosystems), and real-time fluorescence were monitored at an interval of 1 min. End-point fluorescence spectra were carried out on a Shimadzu RF-5301 fluorescence spectrometer (Shimadzu Ltd., Japan) with the excitation at 425 nm and the emission spectra between 450 nm and 600 nm. Excitation and emission slit widths were both set to 5 nm. The optical path length of the quartz fluorescence cell was 1.0 cm.

**Table 1**
The oligonucleotides used in this work.

| Oligonucleotide | Sequence (5′→3′) |
|---|---|
| **T-1** | AAC CCA ACC CGC CCT ACC CAA CCT CAG CAG CAA CAG TGA C |
| **T-2** | AAC CCA ACC CGC CCT ACC CAA CCT CAG CAC AAC GCT ACA ACC TCA GCA GCA ACA GTG AC |
| **T-2s** | AAC CCA ACC CGC CCT ACC CAA CCT CAG CAG CAA CAG TGA CCT CAG CAC AAC GCT ACA A |
| **P** | GTC ACT GTT GCT GCT |
| **P-U** | GTC ACT GTT GCT GC**U** AAA AA*dd*C |
| **HP** | TTT TTT *GAA TTC* GTC ACT GTT GCT GCT *GAA TTC* AAA AAA-P |

The recognition sequences for Nb.BbvCI in **T-1**, **T-2** and **T-2s** are underlined. *dd*C at the 3′-terminus of **P-U** is dideoxycytosine. P at the 3′-terminus of **HP** is phosphorylation. The underlined and italic sequences in **HP** are the recognition sequences of restriction endonuclease EcoRI.

### 2.3. UDG sensor utilizing cross-triggered SDA strategy

A mixture of 100 nM **T-2**, 100 nM **T-2s** and 40 nM **P-U** was prepared in 10 mM Tris-HCl buffer (pH 8.0) consisting of 10 mM $MgCl_2$, 1 mM EDTA and 50 mM NaCl. The mixture was heated at 95 °C for 5 min, then cooled to 25 °C slowly and incubated at 25 °C for 30 min. Next, 0.4 mM dNTPs, 5 μM ThT, 0.5 U Klenow fragment, 2.3 U Nb.BbvCI, 25 U endonuclease IV and varying concentrations of UDG were added. Then, 30 μL of the reaction mixture was incubated at 37 °C in the ABI StepOne Plus real-time PCR system (Applied Biosystems), and fluorescence were recorded at 1 min intervals.

### 2.4. Cell culture and sample preparation

HeLa cells were grown in Dulbecco's modified Eagle's medium (DMEM), supplemented with penicillin 100 U/mL, streptomycin 100 μg/mL and 10% fetal bovine serum and maintained at 37 °C in a humidified atmosphere of 5% $CO_2$ and 95% air. Approximately $1 \times 10^7$ cells were dispensed in a 1.5 mL centrifuge tube, washed twice with PBS buffer and centrifuged at 2000 rpm for 3 min to discard the buffer. A volume of 500 μL lysis buffer (20 mM Tris with a pH value of 7.5, 150 mM NaCl, 1% Triton X-100, sodium pyrophosphate, β-glycerophosphate, EDTA, $Na_3VO_4$ and leupeptin) was added into the cell residues and incubated on ice for 30 min, with vortex for 15 s every 5 min. The resulting mixture was centrifuged at 12,000 rpm for 20 min at 4 °C. The supernatant could be used immediately for UDG activity assay or frozen at −80 °C for long-term storage.

### 2.5. EcoRI sensor utilizing cross-triggered SDA strategy

The EcoRI activity-sensing amplification reaction mixtures were prepared separately as Mix A and Mix B. Mix A (20 μL) contained **HP** (50 nM) in 1 × NEBuffer 2 was incubated at 95 °C for 5 min and then cooled to 25 °C to form the hairpin structures. Variable amounts of EcoRI were added into Mix A. The assay was performed with incubations lasting 2 h at 37 °C before initiating the SDA. Mix B (20 μL) contained 100 nM **T-2**, 100 nM **T-2s** and 1 × NEBuffer 2. Next, Mix A, Mix B, 0.4 mM dNTPs, 5 μM ThT, 0.5 U Klenow fragment polymerase and 2.3 U Nb.BbvCI were mixed to a final volume of 50 μL. Then, 30 μL of the reaction mixture was incubated at 37 °C in the ABI StepOne Plus real-time PCR system (Applied Biosystems), and fluorescence curves were recorded at 1 min intervals.

## 3. Results and discussion

### 3.1. ThT/G-quadruplex-based real-time monitoring of traditional SDA reactions

The working mechanism of the proposed ThT/G-quadruplex-based real-time SDA reaction is in Fig. 1. The DNA oligonucleotides **T-1** and **P** were the template and primer, respectively. **T-1** was designed with three regions: region I hybridized with primer **P**, region II provided a recognition and nicking site for the nicking endonuclease Nb. BbvCI, and region III was a C-rich sequence whose complementary G-rich sequence folded into the G-quadruplex. Hybridization between **T-1** and **P** initiated nicking-polymerization-displacement cycles of the SDA reaction. Thus, the

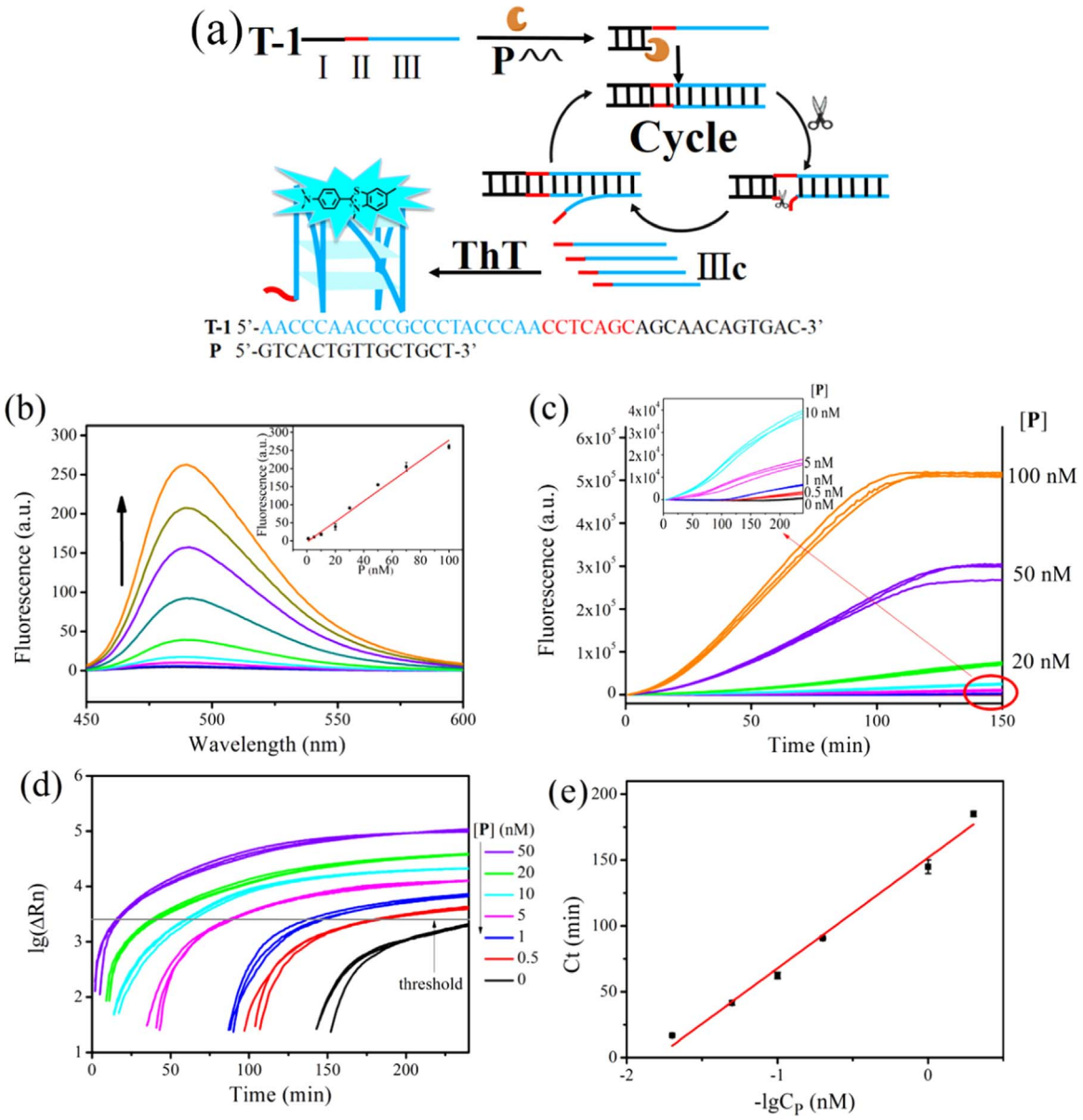


**Fig. 1.** (a) Working mechanism of ThT/G-quadruplex-based linear SDA reaction. DNA sequences drawn in the same color are either identical or complementary. (b) End-point fluorescence spectra of ThT/G-quadruplex-based SDA systems containing various concentrations of **P** (0, 1, 5, 10, 20, 30, 50, 70, 100 nM). The insert shows the linear relationship between fluorescence intensity at 487 nm and the concentration of **P**. (c) Fluorescence∼time curves obtained in real-time SDA. (d) lg(ΔRn)∼time curves. (e) Linear relationship between $RT_t$ values and the negative logarithm of **P** concentration.

extended product of **P** was nicked at the recognition site of Nb. BbvCI. The 3′-end of the upstream part was extended, displacing the downstream part (IIIc). As a result, G-rich IIIc strands were produced through linear amplification. The enrichment of IIIc could be monitored in real-time as the specific response of the fluorescent dye ThT to G-quadruplexes formed by product IIIc.

As a first step, we investigated if ThT could be used to detect SDA products using an end-point detection mode with ThT added after the SDA reactions. Noticeable fluorescence was observed when the dye was mixed with SDA reaction products. Extremely low fluorescent intensities were observed for blank controls in which SDA reactions were not initiated because a necessary component was lacking (Fig. S1). This result demonstrated the high recognition specificity of ThT for DNA G-quadruplexes. As long as templates, primers and undesired amplification products did not fold into G-quadruplexes, low background fluorescence was ensured, providing sensing platforms with high detection sensitivity. To further determine if fluorescence enhancement was closely related to SDA product enrichment, the signal responses of ThT to reaction systems containing different concentrations of primer **P** were recorded. An increase in fluorescence intensity dependent on **P** concentration was observed (Fig. 1b). A linear relationship ($R^2$=0.9963) between fluorescence intensity at 487 nm and **P** concentration was observed in the range of 1–100 nM. If the proposed method was used for quantitation of target DNA **P**, the detection limit (3σ/slope) was estimated to be 0.34 nM.

After demonstrating a rapid fluorescence response time (less than 8 s, Fig. S2) of ThT to SDA amplification products and determining that ThT had no effects on SDA amplification efficiency (Fig. S3), we investigated the feasibility of real-time SDA monitoring. No fluorescence change was observed for blank controls without **P** primer strands. With the addition of **P**, however, time-dependent fluorescence enhancement was observed. Fluorescence enhancement was also dependent on **P** concentration. Higher **P** concentrations gave faster fluorescence changes. These results

demonstrated real-time SDA monitoring using the proposed ThT/G-quadruplex strategy.

The feasibility of applying real-time SDA to biosensor design was investigated. Real-time SDA fluorescence time curves were generated (Fig. 1c), demonstrating a unique data-processing method that is commonly used in real-time PCR. We constructed $\lg(\Delta R_n)$ time curves (with $\Delta R_n$ the fluorescence difference between the reporter fluorophore and the baseline set by the instrument). Thus, target quantitation could be achieved according to the relationship between $RT_t$ value and the logarithm of target concentration, where $RT_t$ was the reaction time when $\lg(\Delta R_n)$ reached a set threshold. This data-processing method might confer sensing platforms with higher detection sensitivity than end-point detection methods. Differences in end-point fluorescence signals between the reaction system containing 0.5 nM **P** and the blank control were small (Fig. 1b). However, a clear difference was observed in $\lg(\Delta R_n)$ time curves (Fig. 1d). A linear relationship ($R^2=0.9967$) was observed for $RT_t$ and $\lg C_P$ in the range of 0.5–50 nM and the detection limit was estimated to be 0.13 nM. Because of the advantages of real-time PCR for biosensing and clinical diagnosis, commercially available real-time PCR instruments are commonly used in biological and clinical laboratories. Our proposed real-time SDA worked on commercial real-time PCR instruments, making high-throughput real-time monitoring of SDA reactions possible. This feature may also help with rapid promotion of the method.

### 3.2. ThT/G-quadruplex-based real-time monitoring of exponential SDA reactions

Traditional SDA reactions follows a linear amplification mechanism. We demonstrated that amplification efficiency was greatly improved using an exponential cross-triggered SDA strategy (Du et al., 2016). Two templates, **T-2** and **T-2s**, were used. In these templates, region I and region IV were exchanged. Each contained two Nb.BbvCI recognition sites. The working mechanism of the cross-triggered SDA reaction is in Fig. 2a. Upon hybridization with template **T-2**, primer **P** initiated the first amplification cycle (Cycle 1) of the SDA reaction, resulting in a linear amplification of IVc and G-rich IIIc. The newly formed strand IVc subsequently hybridized with region IV of **T-2** to trigger the second cycle (Cycle 2). Crucially, IVc also hybridized with template **T-2s** to initiate the third cycle (Cycle 3), giving amplification products Ic and IIIc. The released Ic triggered the fourth cycle (Cycle 4) and provided a new primer for Cycle 1. Since primers for Cycle 1 and Cycle 3 were produced by the cycles, cross-triggered amplification cycles were initiated. All four cycles generated the amplified product IIIc. Therefore, the cross-triggered amplification strategy exponentially enriched for G-rich IIIc strands, which could improve the sensitivity of SDA-based sensing platforms.

The feasibility of real-time monitoring of exponential SDA amplification reactions was investigated. Fluorescence-time curves were obtained that were dependent on both primer concentration and reaction time (Fig. S4). For the real-time SDA-based sensing

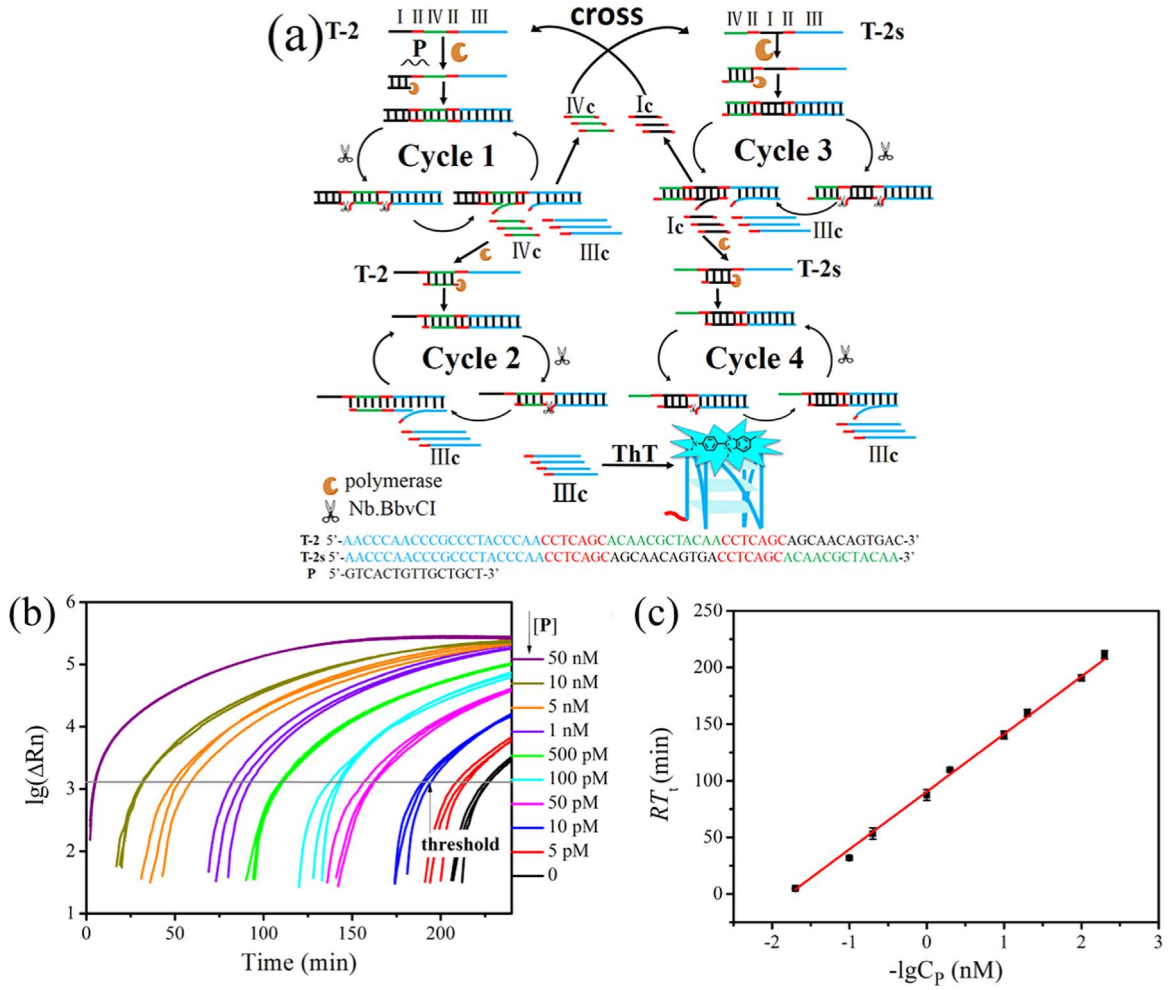


**Fig. 2.** (a) Working mechanism of ThT/G-quadruplex-based cross-triggered SDA reaction. (b) lg(ΔRn)~time curves obtained in real-time SDA. (c) Linear relationship between $RT_t$ values and the negative logarithm of **P** concentration.

platform for target **P** detection, a linear relationship ($R^2$=0.9925) between $RT_t$ value and lg$C_P$ was obtained in the range of 5 pM–50 nM with an estimated detection limit of 1.4 pM. Compared with the sensing platform based on linear SDA amplification reactions, this platform had much higher detection sensitivity. In addition, the linear detection range was expanded since reaction systems gave detectable fluorescence signal changes at lower **P** concentrations.

### 3.3. Biosensors based on real-time cross-triggered SDA

Based on the developed real-time monitoring strategy for SDA reactions, two sensing platforms were developed to demonstrate the application potential of this strategy for biosensor design. The first approach was used to detect UDG. Base-excision repair (BER) is important in maintaining genetic integrity. It removes damaged bases that otherwise cause mutations by mispairing or leading to breaks in DNA during replication (Kunkel and Erie, 2005; Seal et al., 1988; Zharkov et al., 2010). In DNA BER, UDG is a key initiator that specifically removes undesired uracil bases in uracil-containing DNA (Cole et al., 2010; Savva et al., 1995). The development of a highly sensitive and specific sensing platform for UDG activity analysis is of fundamental importance.

The working mechanism of the proposed UDG-sensing platform is in Fig. 3a. **T-2** and **T-2s** were used as templates for cross-triggered SDA reactions. The uracil-containing oligonucleotide **P-U** was used as the primer. **P-U** was designed based on **P**, with the T base at the 3′-end of **P** replaced by the ribonucleic acid base U. **P-U**

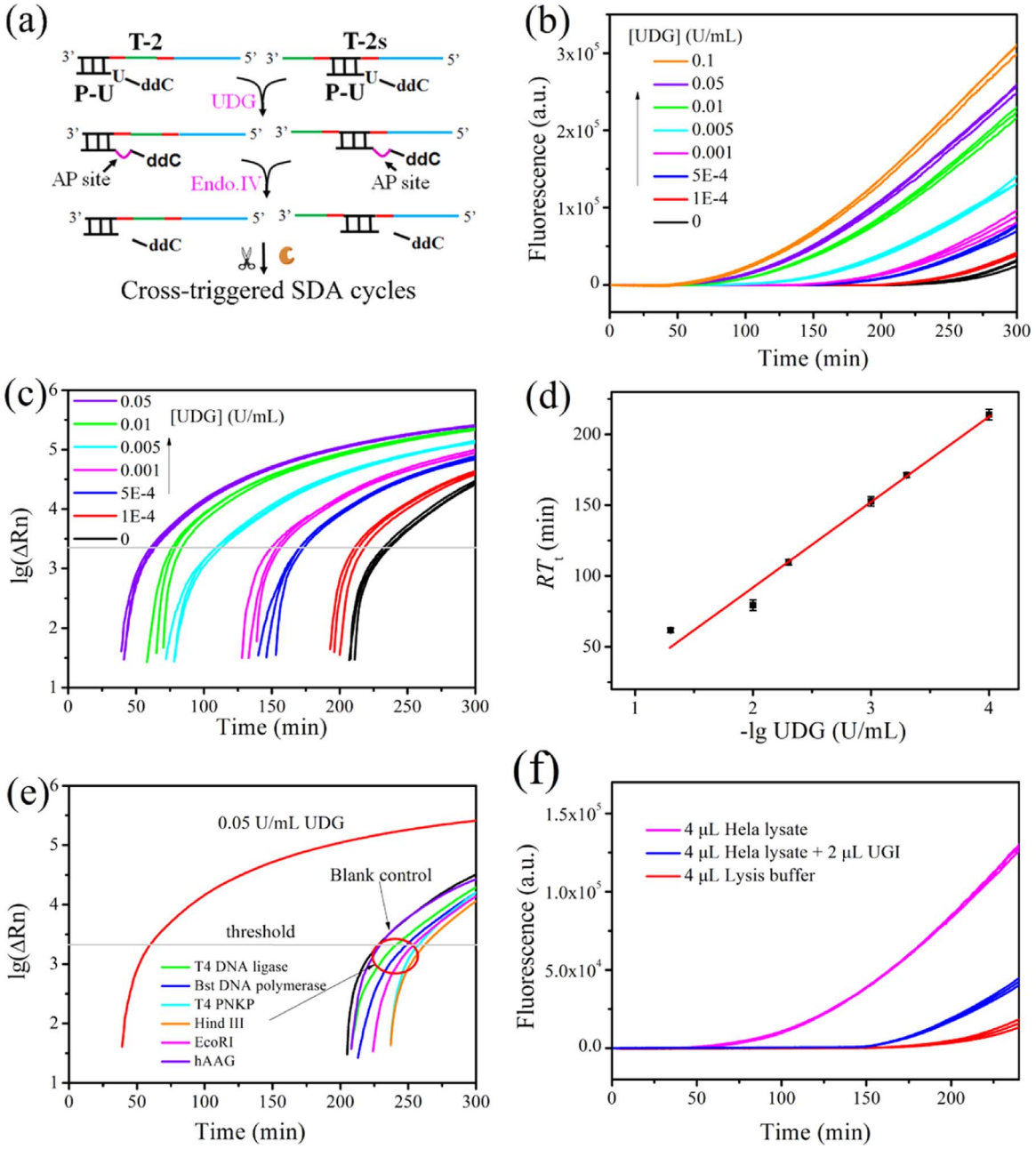


**Fig. 3.** (a) Working mechanism of the proposed UDG-sensing platform. U denotes the uracil ribonucleotide. (b) Fluorescence∼time curves for the systems containing different concentrations of UDG. (c) Corresponding lg(ΔRn)∼time curves. (d) Linear relationship between $RT_t$ values and the negative logarithm of UDG concentration in the range of $1\times10^{-4}$–0.05 U/mL. (e) Selectivity of UDG-sensing system against non-target enzymes (1 U/mL human alkyl adenine DNA glycosylase (hAAG), 1 U/mL T4 DNA ligase, 1 U/mL Bst DNA polymerase, 1 U/mL T4 polynucleotide kinase (PNKP), 1 U/mL restriction endonuclease EcoRI, and 1 U/mL restriction endonuclease Hind III) (f) Fluorescence∼time curves of HeLa cell lysates, and the inhibitory effect of UGI on UDG activity in the cell lysates.

also had an overhang containing five A bases and a dideoxynucleotide-modified C base at the 3′-end. This design disabled **P-U** as a primer for initiating cross-triggered SDA reactions in the absence of UDG. However, treatment of **T-2**/**P-U** and **T-2s**/**P-U** duplexes with UDG resulted in removal of the uracil base, generating an abasic site for subsequent cleavage by endonuclease IV (Endo. IV). The remaining part of **P-U** had a 3′-hydroxyl end for use as the primer for initiating subsequent cross-triggered SDA reactions. The amplification product IIIc folded into G-quadruplexes that could be detected in real time by ThT.

Different concentrations of UDG were added to the sensing systems and SDA amplification reactions monitored in real time (Fig. 3b). According to obtained lg($\Delta R_n$) time curves (Fig. 3c), a linear relationship ($R^2$=0.9962) was observed between $RT_t$ and the logarithm of UDG concentration in the range of $1\times10^{-4}$ to 0.05 U/mL (Fig. 3d). Based on 3σ/slope, the detection limit was calculated to be $6\times10^{-5}$ U/mL. This sensitivity was better than or comparable to previously reported methods (Table S1) (Hu et al., 2011; Liu et al., 2014; Nie et al., 2015; Xiang and Lu, 2012; Zhang et al., 2012; Zhou et al., 2013). The high sensitivity was attributed to synergy between the high amplification ability of the cross-triggered exponential amplification reactions, high sensitivity and specificity for recognizing G-quadruplexes by ThT, and the unique data-processing method of real-time SDA. The proposed platform gave excellent UDG detection selectivity since none of the tested nontarget enzymes had detectable signal increases compared to blank controls (Fig. S5); $RT_t$ values were higher than for $1\times10^{-4}$ U/mL UDG even at $10^4$-fold higher concentrations (Fig. 3e). The selectivity originated from the specific ability of UDG to remove uracil from DNA and the specific fluorescent recognition of G-quadruplexes by ThT.

To investigate whether the UDG sensor worked in cellular environments, we detected UDG activity in HeLa cell lysates. Addition of HeLa lysates induced fluorescence enhancement (Fig. 3f). To determine if the observed fluorescence enhancement was caused by active UDG in the cell lysates, the UDG inhibitor UGI, which had no effect on SDA amplification in primer **P**-initiated cross-triggered SDA reactions, was added in the cell lysates. Inhibition of UDG activity by UGI reduced the signal enhancement in real-time SDA. According to the lg($\Delta R_n$) time curve obtained by taking the logarithm of the fluorescence-time curve difference between systems without and with UGI, UDG activity in HeLa cell lysates was 0.31 U per 1 mg total protein, comparable to results in Xiang et al. (Tao et al., 2015).

To determine the versatility of real-time cross-triggered SDA for biosensing applications, we established another sensing platform for analysis of restriction endonuclease activity. Restriction endonucleases recognize and cleave double-stranded DNA at specific sites (Pingoud and Jeltsch, 2001). These enzymes are essential in recombinant DNA procedures for molecular cloning, analysis of nucleic acids, DNA-protein interaction studies, and antimicrobial and antiviral drug development (Guttman et al., 2002). Therefore, the development of sensitive methods for reliable analysis of endonuclease activity is important for biotechnology and drug discovery. The restriction endonuclease EcoRI is widely used in DNA mutation diagnosis, nucleic acid analysis, and DNA recombination and replication (Roberts, 1990). Using EcoRI as a model analyte, the feasibility of applying real-time SDA to sensitive endonuclease activity sensing was determined. The working principle of the proposed EcoRI sensor is in Fig. S6a. A stem-loop structure substrate (**HP**) with 3′-end phosphorylation modification was used. An EcoRI recognition site was embedded in the double-stranded stem. Upon treatment with EcoRI, specific DNA cleavage released a single-stranded loop sequence that was the primer for initiating cross-triggered SDA reactions. Enrichment of G-rich products was monitored in real time by ThT. Using the sensing platform, EcoRI activity in the range of 0.05–5 U/mL was quantified with a detection limit of 0.016 U/mL (Fig. S6). This detection sensitivity was better than or comparable to reported assays for EcoRI detection (Table S2). In addition to sensitivity, the sensing platform was highly specific for EcoRI versus other restriction endonucleases with different recognition sites. In addition, the proposed method worked well in biological samples (Fig. S7). We noted that $RT_t$ value exhibits good linear correlation with the logarithm of EcoRI activity, even in human serum, indicating the potential applications in a biological system. By adjusting the restriction endonuclease recognition sequences in the double-stranded stem of **HP**, this sensor design strategy could be easily extended to analysis of other restriction endonucleases.

## 4. Conclusion

In summary, a label-free method was developed for real-time monitoring of SDA reactions by incorporating G-quadruplex structures in amplification products. The method used specific recognition of G-quadruplexes by the fluorescent probe ThT. We demonstrated that the method could be used for real-time monitoring of traditional SDA reaction and cross-triggered SDA reaction with exponential amplification efficiency. These results indicated that the method was suitable for construction of biosensing platforms. As examples, two highly sensitive and specific biosensors were designed to analyze the activity of UDG and EcoRI. Detection limits were as low as $6\times10^{-5}$ U/mL for UDG and 0.016 U/mL for EcoRI. Using these sensors, detection of targets in complex matrix such as cell lysates and human serum was possible. Compared to end-point detection methods, real-time SDA-based approaches have the following advantages. (1) They eliminate the need for postamplification detection of products, simplifying the procedures. (2) SDA reactions and product detection are synchronous. Reaction tubes could be discarded without opening, reducing the possibility of carryover contamination. This feature is particularly important for exponential nucleic acid amplification reactions. (3) Closed-tube assays give reliable and reproducible results. (4) The proposed real-time monitoring strategy worked on commercial real-time PCR instruments, making high-throughput detection of up to 96 target samples possible. If conducted on a fluorescent scanner, the analytical throughput might be further increased, and the needs for complicated instruments are also eliminated. (5) Using the fluorescence∼time curves obtained in real-time SDA, a unique signal-processing mode could be performed. This mode might increase the dynamic detection range and detection sensitivity to some degree. Overall, the introduction of a real-time monitoring strategy could promote the application of SDA reactions in biosensor design.

## Acknowledgment

This work was supported by the National Natural Science Foundation of China (Nos. 21322507 and 21371130), and the National Natural Science Foundation of Tianjin (No. 16JCYBJC19900).

## Appendix A. Supplementary material

Supplementary data associated with this article can be found in the online version at http://dx.doi.org/10.1016/j.bios.2016.07.083.

## References

Balasubramanian, S., Hurley, L.H., Neidle, S., 2011. Nat. Rev. Drug Discov. 10,

261–275.
Bustin, S.A., Benes, V., Nolan, T., Pfaffl, M.W., 2005. J. Mol. Endocrinol. 34, 597–601.
Chen, A., Gui, G.-F., Zhuo, Y., Chai, Y.-Q., Xiang, Y., Yuan, R., 2015a. Anal. Chem. 87, 6328–6334.
Chen, Y., Song, Y., Wu, F., Liu, W., Fu, B., Feng, B., Zhou, X., 2015b. Chem. Commun. 51, 6980–6983.
Cole, H.A., Tabor-Godwin, J.M., Hayes, J.J., 2010. J. Biol. Chem. 285, 2876–2885.
Deng, M., Zhang, D., Zhou, Y., Zhou, X., 2008. J. Am. Chem. Soc. 130, 13095–13102.
Du, Y.-C., Jiang, H.-X., Huo, Y.-F., Han, G.-M., Kong, D.-M., 2016. Biosens. Bioelectron. 77, 971–977.
Gao, Y., Li, B., 2014. Anal. Chem. 86, 8881–8887.
Guttman, A., Ronai, Z., Barta, C., Hou, Y.-M., Sasvari-Szekely, M., Wang, X., Briggs, S. P., 2002. Electrophoresis 23, 1524–1530.
Hu, D., Huang, Z., Pu, F., Ren, J., Qu, X., 2011. Chem. Eur. J. 17, 1635–1641.
Huang, X.-X., Zhu, L.-N., Wu, B., Huo, Y.-F., Duan, N.-N., Kong, D.-M., 2014. Nucleic Acids Res. 42, 8719–8731.
Huang, Y., Liu, X., Huang, H., Qin, J., Zhang, L., Zhao, S., Chen, Z.-F., Liang, H., 2015. Anal. Chem. 87, 8107–8114.
Huang, Y.C., Sen, D., 2015. Angew. Chem. Int. Ed. 53, 14055–14059.
Jia, H., Li, Z., Liu, C., Cheng, Y., 2010. Angew. Chem. Int. Ed. 49, 5498–5501.
Jiang, Y., Li, B., Milligan, J.N., Bhadra, S., Ellington, A.D., 2013. J. Am. Chem. Soc. 135, 7430–7433.
Jiang, H.-X., Kong, D.-M., Shen, H.-X., 2014. Biosens. Bioelectron. 55, 133–138.
Jiang, H.-X., Zhao, M.-Y., Niu, C.-D., Kong, D.-M., 2015. Chem. Commun. 51, 16518–16521.
Kunkel, T.A., Erie, D.A., 2005. Annu. Rev. Biochem. 74, 681–710.
Li, D., Wieckowska, A., Willner, I., 2008. Angew. Chem. Int. Ed. 47, 3927–3931.
Li, W., Liu, Z., Lin, H., Nie, Z., Chen, J., Xu, X., Yao, S., 2010. Anal. Chem. 82, 1935–1941.
Li, C., Qiu, X., Hou, Z., Deng, K., 2015a. Biosens. Bioelectron. 64, 505–510.
Li, F., Zhang, H., Wang, Z., Newbigging, A.M., Reid, M.S., Li, X.-F., Le, X.C., 2015b. Anal. Chem. 87, 274–292.
Liu, X., Chen, M., Hou, T., Wang, X., Liu, S., Li, F., 2014. Biosens. Bioelectron. 54, 598–602.
Mohanty, J., Barooah, N., Dhamodharan, V., Harikrishna, S., Pradeepkumar, P.I., Bhasikuttan, A.C., 2013. J. Am. Chem. Soc. 135, 367–376.
Nie, H., Wang, W., Li, W., Nie, Z., Yao, S., 2015. Analyst 140, 2771–2777.
Nilsson, M., Gullberg, M., Dahl, F., Szuhai, K., Raap, A.K., 2002. Nucleic Acids Res. 30, e66.
Patel, D.J., Phan, A.T., Kuryavyi, V., 2007. Nucleic Acids Res. 35, 7429–7455.
Pingoud, A., Jeltsch, A., 2001. Nucleic Acids Res. 29, 3705–3727.
Roberts, R.J., 1990. Nucleic Acids Res. 18, 2331–2365.
Savva, R., Mcauley-Hecht, K., Brown, T., Pearl, L., 1995. Nature 373, 487–493.
Schmittgen, T.D., Livak, K.J., 2008. Nat. Protoc. 3, 1101–1108.
Seal, G., Brech, K., Karp, S.J., Cool, B.L., Sirover, M.A., 1988. Proc. Natl. Acad. Sci. USA 85, 2339–2343.
Tao, J., Song, P., Sato, Y., Nishizawa, S., Teramae, N., Tong, A., Xiang, Y., 2015. Chem. Commun. 51, 929–932.
Tian, L., Weizmann, Y., 2013. J. Am. Chem. Soc. 135, 1661–1664.
Valasek, M.A., Repa, J.J., 2005. Adv. Physiol. Educ. 29, 151–159.
Wang, F., Lu, C.H., Willner, I., 2014. Chem. Rev. 114, 2881–2941.
Wong, M.L., Medrano, J.F., 2005. Biotechniques 39, 75–85.
Xiang, Y., Lu, Y., 2012. Anal. Chem. 84, 9981–9987.
Yamuna, K., Friedrich, C., 2011. Angew. Chem. Int. Ed. 50, 3124–3156.
Yin, B.-C., Ye, B.-C., Tan, W., Wang, H., Xie, C.-C., 2009. J. Am. Chem. Soc. 131, 14624–14625.
Zhang, L., Zhao, J., Jiang, J., Yu, R., 2012. Chem. Commun. 48, 8820–8822.
Zhang, Z.-Z., Zhang, C.-Y., 2012. Anal. Chem. 84, 1623–1629.
Zhang, P., Wu, X., Yuan, R., Chai, Y., 2015a. Anal. Chem. 87, 3202–3207.
Zhang, Q., Liu, Y.-C., Kong, D.-M., Guo, D.-S., 2015b. Chem. Eur. J. 21, 13253–13260.
Zhao, Y., Chen, F., Li, Q., Wang, L., Fan, C., 2015. Chem. Rev. 115, 12491–12545.
Zharkov, D.O., Mechetin, G.V., Nevinsky, G.A., 2010. Mutat. Res. 685, 11–22.
Zhou, D.M., Xi, Q., Liang, M.F., Chen, C.H., Tang, L.J., Jiang, J.H., 2013. Biosens. Bioelectron. 41, 359–365.
Zhu, L.-N., Wu, B., Kong, D.-M., 2013. Nucleic Acids Res. 41, 4324–4335.